© ESO 2010

GRB 021004: Tomography of a gamma-ray burst progenitor and its host galaxy [*]

A. J. Castro-Tirado[1], P. Møller[2], G. García-Segura[3], J. Gorosabel[1], E. Pérez[1], A. de Ugarte Postigo[4], E. Solano[5], D. Barrado-Navascués[5], S. Klose[6], D. A. Kann[6], J. M. Castro Cerón[7], C. Kouveliotou[8], J. P. U. Fynbo[9], J. Hjorth[9], H. Pedersen[9], E. Pian[2,10,11], E. Rol[12,13], E. Palazzi[14], N. Masetti[14], N. R. Tanvir[12], P. M. Vreeswijk[9], M. I. Andersen[9], A. S. Fruchter[15], J. Greiner[16], R. A. M. J. Wijers[13], and E. P. J. van den Heuvel[13]

[1] Instituto de Astrofísica de Andalucía (IAA-CSIC), Glorieta de la Astronomía s/n, E-18.008 Granada, Spain.
[2] European Southern Observatory, Karl-Schwarzschild-Strae 2, 85748, Garching bei Munchen, Germany.
[3] Instituto de Astronomía, Universidad Nacional Autónoma de México, Apdo. Postal 877, Ensenada 22800, Baja California, México.
[4] INAF, Osservatorio Astronomico di Brera, via E. Bianchi 46, 23807 Merate (LC), Italy.
[5] Laboratorio de Astrofísica Estelar y Exoplanetas, Dpto. Astrofísica, Centro de Astrobiología (CSIC/INTA), P.O. Box 78, 28691 Villanueva de la Cañada (Madrid), Spain.
[6] Thüringer Landessternwarte Tautenburg, Sternwarte 5, D-07778 Tautenburg, Germany.
[7] European Space Agency (ESA), European Space Astronomy Centre (ESAC), P.O. Box - Apdo. de correos 78, 28691 Villanueva de la Cañada, Madrid, Spain.
[8] NASA Marshall Space Flight Center, NSSTC, 320 Sparkman Drive, Huntsville, Alabama 35805, USA.
[9] Dark Cosmology Centre, Niels Bohr Institute, University of Copenhagen, Juliane Maries Vej 30, DK-2100 København Ø, Denmark.
[10] INAF - Osservatorio Astronomico di Trieste, via Tiepolo, 11, 34131 Trieste, Italy.
[11] Scuola Normale Superiore di Pisa, Piazza dei Cavalieri 7, I-56126 Pisa, Italy.
[12] Department of Physics & Astronomy, University of Leicester, University Road, Leicester, LE1 7RH, UK.
[13] Astronomical Institute "Anton Pannekoek", University of Amsterdam, PO number 94249, 1090 GE, Amsterdam, NL.
[14] INAF - IASF di Bologna, via Gobetti 101, I-40129 Bologna, Italy.
[15] Space Telescope Science Institute, 3700 San Martín Dr, Baltimore, MD 21218-2463, USA.
[16] Max-Planck-Institut für extraterrestrische Physik, 85748 Garching, Germany.

ABSTRACT

Aims. Analyse the distribution of matter around the progenitor star of gamma-ray burst GRB 021004 as well as the properties of its host galaxy with high-resolution echelle as well as near-infrared spectroscopy.

Methods. Observations were taken by the 8.2m Very Large Telescope with the Ultraviolet and Visual Echelle spectrograph (UVES) and the Infrared Spectrometer And Array Camera (ISAAC) between 10 and 14 hours after the onset of the event.

Results. We report the first detection of emission lines from a GRB host galaxy in the near-infrared, detecting Hα and the [O III] doublet. These allow an independent measurement of the systemic redshift ($z = 2.3304 \pm 0.0005$) which is not contaminated by absorption as the Lyα line is, and the deduction of properties of the host galaxy. From the visual echelle spectroscopy, we find several absorption line groups spanning a range of about 3,000 km s^{-1} in velocity relative to the redshift of the host galaxy. The absorption profiles are very complex with both velocity-broadened components extending over several 100 km s^{-1} and narrow lines with velocity widths of only $\sim$ 20 km s^{-1}. By analogy with QSO absorption line studies, the relative velocities, widths, and degrees of ionization of the lines ("line-locking", "ionization–velocity correlation") show that the progenitor had both an extremely strong radiation field and several distinct mass loss phases (winds).

Conclusions. These results are consistent with GRB progenitors being massive stars, such as Luminous Blue Variables (LBVs) or Wolf–Rayet stars, providing a detailed picture of the spatial and velocity structure of the GRB progenitor star at the time of explosion. The host galaxy is a prolific star-forming galaxy with a SFR of $\sim$40 M$_\odot$yr^{-1}.

Key words. (Stars:) Gamma-ray bust – Techniques: spectroscopic – Stars: Wolf-Rayet – Galaxies: starburst – Cosmology: observations

1. Introduction

The afterglows of long-duration Gamma-Ray Bursts (GRBs), which are linked with the explosions of massive stars (see

Woosley & Bloom, 2006, for a recent review), are the most luminous optical sources in the universe for short periods of time (Kann et al., 2007; Bloom et al., 2009). Low-resolution optical spectroscopy was initially only usable to determine the redshift and thus place them at cosmological distances (Metzger et al., 1997). Deeper insight came with the first medium-resolution spectrum, obtained with Keck ESI of the afterglow of GRB 000926 (Castro et al., 2003). The first true high-resolution echelle spectra were obtained for GRB 020813 (Fiore et al., 2005), but they were of low signal-to-noise ratio. The first echelle spectra with good S/N were finally obtained for GRB 021004, the focus of this work (see also Fiore et al., 2005).

Such spectroscopy allows deep insight into the environments of GRBs (Prochaska et al., 2006). Some highlights include the possible detection of a Galactic superwind in the host galaxy of GRB 030329 (Thöne et al., 2007), and variable absorption lines which result from direct UV pumping by the luminous GRB afterglow (Dessauges-Zavadsky et al., 2006; Vreeswijk et al., 2007; D'Elia et al., 2009). These detections have recently been possible for more afterglows due to the rapid localization capabilities of the *Swift* satellite (Gehrels et al., 2004) in combination with the rapid-response mode (RRM) which is now available for the Ultraviolet-Visual Echelle Spectrograph (UVES) at the Very Large Telescope (VLT) (e.g., Vreeswijk et al., 2007; D'Elia et al., 2009). Recently, the covered wavelength region has been expanded all the way from the ultraviolet into the K band near-infrared (nIR) by the second-generation instrument X-Shooter at VLT (D'Odorico et al., 2006, see de Ugarte Postigo et al. 2009 for a first result).

GRB 021004 was detected at 12:06:14 universal time (UT) on 2002, October 4 with the gamma-ray instrument FREGATE, the wide-field X-ray Monitor (WXM) and the soft X-ray camera (SXC) aboard the High-Energy Transient Explorer (*HETE-2*) (Shirasaki et al., 2002). GRB 021004, was a moderately bright, long-duration (T_{90} = 100 s) event with fluences of 6.4×10^{-7} erg cm^{-2} (7-30 keV) and 2.3×10^{-6} erg cm^{-2} (30-400 keV) (Barraud et al., 2002).

The GRB was rapidly localized in flight and the position was reported in less than a minute, allowing rapid ground-based follow-up which revealed the presence of the fading optical afterglow of GRB 021004 (Fox et al., 2003). This prompted follow-up observations at many observatories, which led to an extensive long-term coverage at X-ray Sako & Harrison (2002a,b), radio (Frail & Berger, 2002; Berger et al., 2002; Pooley, 2002a,b)[1], millimeter (de Ugarte Postigo et al., 2005), near-IR (de Ugarte Postigo et al., 2005; Fynbo et al., 2005) and optical wavelengths, both ground-based (Fox et al., 2003; Bersier et al., 2003; Uemura et al., 2003; Holland et al., 2003; Pandey et al., 2003; Mirabal et al., 2003; Kawabata et al., 2004; de Ugarte Postigo et al., 2005) as well as space-based (Fynbo et al., 2005).

The isotropic energy release during the prompt emission of this GRB was modest, with log $E_{iso} = 52.65^{+0.12}_{-0.17}$ (Kann et al., 2010), and the dust extinction for this somehow reddish afterglow (R-K ~ 3) was also low as is typical for many well-

observed afterglows (Kann et al., 2006). Despite the low energy promptly released, this is among the most luminous afterglows ever detected (Kann et al., 2006), even in comparison with a much larger *Swift*-era sample (Kann et al., 2010). The multiwavelength temporal evolution of the GRB 021004 afterglow can be explained by multiple energy injections (Björnsson et al., 2004; de Ugarte Postigo et al., 2005), nevertheless other scenarios can not be discarded (Lazzati et al., 2002). GRB 021004 remains one of the most well-observed afterglows ever.

Early-time low and medium resolution spectroscopic observations allowed a redshift of z = 2.33 to be determined on the basis of Ly-α absorption and emission lines (Chornock & Filippenko, 2002). Several absorption systems with outflows velocities of few 1000 km s^{-1} were also reported (Salamanca et al., 2002; Savaglio et al., 2002) and studied in detail by Møller et al. (2002b), Wang et al. (2003), Matheson et al. (2003), Schaefer et al. (2003), Mirabal et al. (2003), Starling et al. (2005) and Lazzati et al. (2006). Jakobsson et al. (2005) also report the detection of the host galaxy Lyα line in narrow-band imaging.

Fiore et al. (2005) have constrained the ionization parameters of the various absorption components detected above Lyα (at an observer restframe of 4,050 Å) in GRB 021004, interpreting them as density fluctuations, like Lazzati et al. (2002) did. Within the context of larger samples, the UVES spectra of this GRB have also been studied by Chen et al. (2007) (the general lack of wind signatures in high-resolution spectra of GRB afterglows), Prochaska et al. (2008) (N V absorption lines toward GRB afterglows), Fox et al. (2008) (high-ionisation line systems toward GRB afterglows) and Tejos et al. (2007, 2009); Vergani et al. (2009) (study of Mg II foreground absorption systems).

The original expectation, as detailed high quality spectroscopy of GRB afterglows became possible, was that we would rapidly learn much about the GRB progenitors via the study of the complex absorption line systems they were expected to exhibit due to ejection events leading up to the final collapse. This expectation has far from proven true.

Despite the large number of long GRB afterglow spectra obtained since, GRB 021004 still stands out as the one with the most complex set of intrinsic (0-3,000 km/s ejection velocity) absorption systems. At the time it also held the place as the lowest detected HI column density, and it still ranks between the lowest seven found. The complexity originally suggested that it indeed represented a display of ejecta (Møller et al., 2002a; Mirabal et al., 2003; Fiore et al., 2005) but this interpretation was later disputed by Chen et al. (2007). A final interpretation of the complex systems has not yet been agreed on, and this object still stands our as the best candidate of a seemingly rare case where the signatures of events prior to the collapse are displayed. The rarity alone would warrant a more detailed discussion of the spectral features. In addition we are adding UVES data below 4050 ang for a more detailed discussion of the absorption systems (para 3.1) and near-IR VLT/ISAAC spectroscopy allowing a more accurate determination of host properties and redshift (para 3.2). We discuss our results in the

---

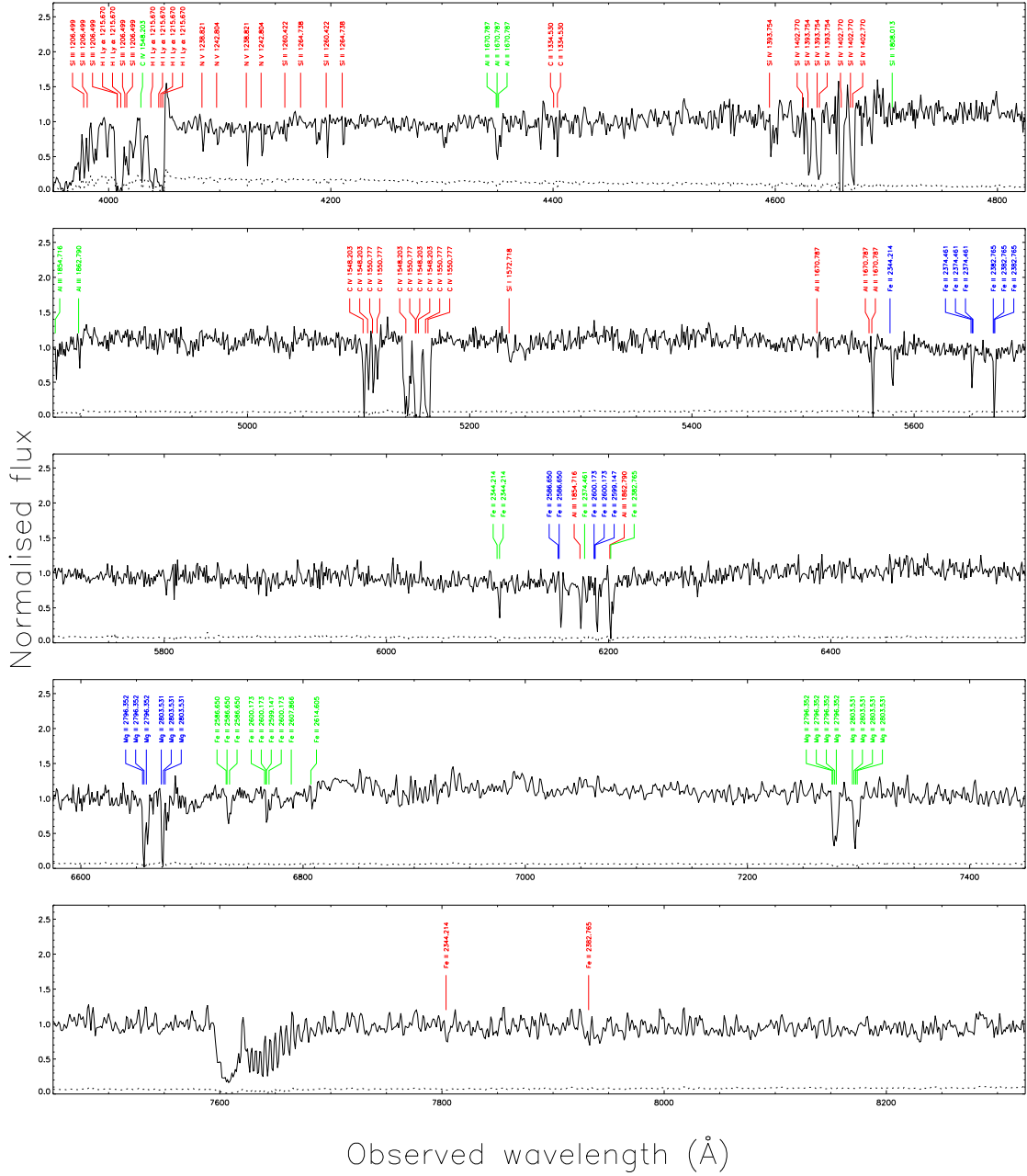[1] See http://www.aoc.nrao.edu/~dfrail/grb021004.dat for the complete VLA data set.

Fig. 1. Overall view of GRB 021004 optical afterglow spectrum. These VLT/UVES data were obtained ~0.6 days after the GRB and show the Lyα emission line arising from the host galaxy redshift plus some of the most prominent absorption lines systems at (or very close to) the host galaxy redshift: low ionization lines (like Fe II, Si II) and high ionization lines (like Si IV, C IV, N V), all labelled in red colour. Also shown for completeness are the absorption systems for the foreground systems at $z = 1.6020$ (labelled in green) and $z = 1.3820$ (labelled in blue). For clarity, the original data have been smoothed. The telluric lines in the A-band (7600–7630 Å) are noticeable. The dotted line is the error spectrum.

light of progenitor models for GRBs in § 4, and summarize the work in § 5.

For a Hubble constant of $H_0 = 72$ km s^{-1} Mpc^{-1}, a matter density $\Omega_m = 0.3$, and a cosmological constant $\Omega_\Lambda = 0.7$, the luminosity distance to the host is $d_L = 18.22$ Gpc, and the lookback time is 10.42 Gyr. All errors are given at a 1σ level of confidence for a parameter of interest unless stated otherwise.

2. Observations and data reduction

2.1. Optical observations

Observations were conducted with 8.2-m Very Large Telescope Units 1 (VLT/UT1, Antu) and 2 (VLT/UT2, Kueyen) at the European Southern Observatory (ESO) in Cerro Paranal (Chile). We obtained optical spectroscopy of the

GRB afterglow starting 0.6 days after the burst using the Ultraviolet-Visual Echelle Spectrograph (UVES) on UT2. Contemporaneous nIR observations were taken using the Infrared Spectrometer And Array Camera (ISAAC) on UT1 (see Table 1 for a log of the observations).

The optical data reduction was performed using the UVES context running under MIDAS[2]. The UVES context is structured into reduction recipes allowing for data reduction in a semi-automatic manner. A master bias frame was used for the bias subtraction. The order tracing was performed taking advantage of a first guess calibration solution based on the UVES physical model. In all cases, except for the red spectrum centered at 8,600 Å which is affected by fringing effects, the flat field correction was applied after the order extraction. A Th-Ar lamp was used for wavelength calibration. The spectra were extracted using an optimal extraction method, which provides the object signal and the variance. After the extraction the spectra were resampled to constant wavelength bins and the orders merged into a single spectrum. Finally, both the standard heliocentric and vacuum wavelength corrections were applied.

2.2. Near-infrared observations

For the nIR observations we used the short wavelength mode in low resolution, which yields a spectral coverage of 1.42-1.83 μm and 1.84-2.56 μm in the H and K bands, respectively. The pixel scale of the ESO-Hawaii detector is 0''.146/pixel. For each band, 50 individual exposures of 60 seconds each were taken, shifting the target along the slit every 5 exposures in H (3 in K) in order to be able to remove the sky background, a standard technique in infrared astronomy. We also collected dark and flat field images, which were used in the reduction process performed with IRAF[3]. After combining the groups of exposures and extracting the individual spectra, we calibrated them using the air-glow OH emission lines present in the 2 dimensional images. This allows an accurate wavelength calibration with dispersion of 4 and 8 Å/pix for H and K respectively. Finally, the individual spectra were median-combined into a single one. In the case of the H band spectrum we used a G2 spectral type star to remove the telluric absorption bands. The spectra were flux calibrated by means of the JHK-band observations that we obtained bracketing the spectral observations.

3. Results

3.1. The blueshifted absorption line systems

The VLT/UVES data set (Fig. 1) shows a large number of absorption lines, as well as Lyα in emission (see Table 3 for a list, and also Møller et al. 2002b; Starling et al. 2005;

Table 1. Journal of the VLT GRB 021004 optical/nIR spectroscopic observations. All observations were obtained on October 5 (UT).

UT Time (start)	Instr.	Exp. time (s)	Spectral Range (Å)	S/N ratio[a]	Resolution $\lambda/\Delta(\lambda)$
03:02	UVES	3600	3290-4520	1	~ 56000
			4620-5595	2.2	~ 51500
			5675-6645	2.7	~ 51500
03:02	ISAAC	3600	14200-18300	5.2	~ 500
04:10	UVES	3600	3050-3870	1	~ 51300
			4780-5755	3.7	~ 50500
			5835-6805	5.4	~ 50500
05:15	UVES	3600	3750-4650	2.4	~ 51500
			6705-8520	4.1	~ 52300
			8665-10400	2.2	~ 48700
05:27	ISAAC	3000	18400-25800	2.3	~ 450

[a] per resolution element.

Table 2. Individual high-velocity metal-lines systems in GRB 021004.

Line ID	C2	C1	D	E2	E1
Si III λ1,206	y [a]	y	y	y	y
H I Lyα λ1,216	y	y	y	y	y
N V λ1,238-1,242	y	–	–	–	y
Si II λ1,260-1,264	–	y	?	–	y
C II λ1,334	y	y	–	–	–
Si IV λ1,394-1,403	?	?	?	?	y
C IV λ1,548-1,551	y	y	y	y	y
Al II λ1,671	–	y	–	y	y
Al III λ1,855-1,863	–	–	–	–	y
Fe II λ2,344-2,382	–	–	–	–	y
z	2.29671	2.29935	2.3216	2.3275	2.32891
v (km/s)[b]	−3,050[c]	−2,810[d]	−795[e]	−262[f]	−134[g]

[a] y = yes; − = no; ? = doubtful, low significance due to low S/N ratio in the S IV region.
[b] relative to the systemic velocity of the host galaxy at z = 2.3304, which we set as zero.
[c] Embedded as C1 in the wide C complex (2,730-3,250 km s^{-1}).
[d] Two subcomponents at −2,837 and −2,803 km s^{-1} (low ionization) and −2,860 and −2,810 km s^{-1} (high ionization).
[e] Wide complex spanning 585-1,005 km s^{-1}.
[f] Embedded as E1 in the wide E complex (40-390 km s^{-1}).
[g] Two subcomponents at −150 and −114 km s^{-1}.

Jakobsson et al. 2005 on the Lyα emission line). Some of the absorption lines are due to two foreground systems at redshifts $z = 1.3820$ and $z = 1.6020$ (Møller et al., 2002b; Mirabal et al., 2003, see Tejos et al. 2007, 2009; Vergani et al. 2009 for further discussions on the foreground absorbers), but the remaining lines are from multiple systems found in the redshift range $2.2967 \leq z \leq 2.3291$.

In Fig. 2 we show the three wide absorption line complexes in the redshift range $2.2967 \leq z \leq 2.3291$. The absorption profiles are plotted in velocity space and marked C, D, and E following the naming convention used by Møller et al. (2002a). The higher resolution of the UVES spectrum allowed us to

identify four narrow line systems embedded inside the velocity structure of the broad systems C and E. We name those systems C1, C2, E1 and E2. In the following we discuss all of those systems in more detail in order of increasing velocity relative to the host redshift ($z = 2.3304$, see § 3.2).

E complex: The Lyα absorption width translates to velocities in the range 40–470 km s^{-1}, while in C IV (where we observe the narrowest trough), the range is 40–390 km s^{-1}. The difference in the high-velocity cut-offs (390 vs. 470 km s^{-1}) is most easily understood as a column density effect, i.e., the column density of the high velocity end is too low for C IV to be detectable. Alternatively it could be caused by lower metallicity in the higher velocity gas of system E, or a different ionization. The simplest interpretation of the E complex is that it is caused by gas, spanning velocities from 40–470 km s^{-1} and densities decreasing from the slowest to the fastest moving part. Similar profiles have been observed in QSO broad absorption line (BAL) systems, where velocities up to $\approx 0.1c$ have been found. BAL systems are interpreted as velocity broadening due to ejection and/or radiative acceleration. Such BAL-like absorption troughs are not meaningfully fitted by standard (Voigt) profiles that assume a Gaussian velocity field.

Embedded in the E complex are two narrow line systems at 134 km s^{-1} (E1) and 262 km s^{-1} (E2). The strongest component, E1, splits equally into two subcomponents at 114 km s^{-1} and 150 km s^{-1} (see Fig 3) and exhibits absorption from a large number of both high and low ionic species (N V, C IV, Fe II, Al II, Al III, Si II, Si III, Si IV). The metal line absorption of E1 has similarities to so-called damped Lyα (DLA) systems, which in a few cases have been identified with high redshift, star forming galaxies (Møller et al., 2002b) but it has too low HI column density in this sightline to be considered a DLA. Still, E1 is the system most likely to be identified with the interstellar medium (ISM) in the host galaxy of the GRB, whereby the velocity offset between the host and the ISM (~ 134 km s^{-1}) represents the velocity of the local absorbing cloud within the host. High and low ionic species are also seen in the second system (E2), but at lower significance. The two rightmost dotted vertical lines in Fig 2 mark the systems E1 and E2.

D Complex: The D complex consists of a single, wide BAL-like component seen in Lyα, C IV, and Si III. Both the C IV (1,548 Å) and the Lyα troughs give a consistent relative velocity range from 585 to 1,005 km s^{-1}. We find residual flux at the bottom of both the Lyα and C IV (1,548 Å) troughs indicating that the gas is optically thin. We also see significant variations in the optical thickness as a function of relative velocity; in particular one will notice the two sharp "dips" marking shells of higher column density at the leading and the trailing edge. Those dips are seen in Lyα, in both C IV lines and in Si III (marked by dotted lines in Fig 2). The Si III trough is optically thick between those two edges, but then appears to have an optically thin extension towards lower ejection velocities. However, this trough overlaps with Lyα of system C, and the extension is found to belong to system C (see below). .

It is remarkable that the D and E systems are separated in velocity by exactly the amount required to shift the C IV 1,550 Å line complex right on top of the C IV 1,548 Å one in the spectrum (Møller et al., 2002b; Savaglio et al., 2002). Such a shift is known as absorption-absorption "line-locking" and is not uncommon in QSO spectra where radiative acceleration is important (e.g., Srianand et al. 2002). The line-locking between the D and E systems strongly suggests that a process similar to that seen in intrinsic QSO absorption systems is indeed involved here, i.e. radiative acceleration.
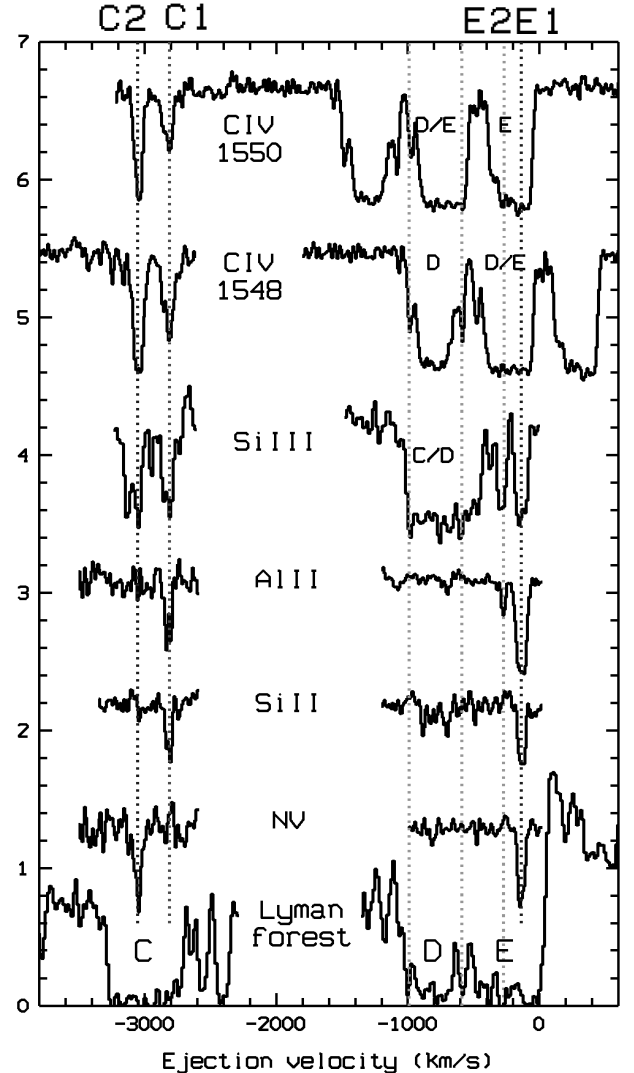

Fig. 2. In this figure we have converted the observed wavelengths into velocities relative to the host redshift ($z = 2.3304$) for each ionic species significantly detected. Lyα is plotted at the bottom. To optimize the signal-to-noise ratio two lines of N V (1,238 and 1,242 Å) and four lines of Si II (1,260, 1,264, 1,533 and 1,816 Å) have been coadded. The rest of the lines are all single. The absorption components around $z \sim 2.3$ observed at velocities up to 3,250 km s^{-1} indicate the presence of fast winds, ejected by a hot and massive stellar progenitor. The D and E complexes both contain velocity broadened, BAL-like components. Within the E complex there are narrow lines, E1 and E2, presumably from the ISM of the host galaxy. There are also narrow shells in the high-velocity system C, C1 and C2. The dotted lines mark the positions of E1, E2, the "dips" at the leading and the trailing edges of D, and the C1 and C2 systems.

C Complex: As discussed above, the wide Lyα trough of system C is partly due to Si III absorption from system D, but also contains Lyα absorption of a wide component spanning the velocity range 2,730–3,250 km s^{-1} as we detect C II, C IV, Si II, Si III, Al II and N V absorption in this velocity range (Fig. 2). The finely tuned velocity offset which causes a precise overlap between the Lyα (C complex) and Si III (D complex) lines could be due to chance coincidence (although with small probability, see below). Given the evidence for line-locking between the two C IV lines between systems D and E, the overlap is most likely the result of radiative acceleration leading to line-locking of two expanding shells corresponding to the C and D complexes.

Embedded in C we identify two narrow systems at 3,050 km s^{-1} (C2) and at ∼ 2,810 km s^{-1} (C1). C2 is a high ionisation system displaying strong N V and C IV absorption, but no absorption from singly ionized ions. C1 is a low ionization system with moderate C IV absorption and clear detections of the singly ionized species Al II and Si II, which usually identifies a cloud optically thick at the Lyman limit (see Table 3). Most likely C2, although farthest away from the host redshift in velocity space, corresponds to the part of the wind that is nearest to the progenitor site in physical space. This ionization–velocity correlation is also observed in QSOs: the high ionization lines are often seen at the highest relative velocities for the $z_{abs} \approx z_{em}$ absorption systems in QSO spectra (e.g., Møller et al. 1994). As for E1, C1 splits into two subcomponents, detected at 2,803 km s^{-1} and 2,837 km s^{-1} (low ionization) and at 2,810 km s^{-1} and 2,860 km s^{-1} (high ionization). Again, we here have the ionization-velocity correlation seen already between C1 and C2 (Fig. 2). Similarly to Fiore et al. (2005) we do consider C1 as part of the ejected systems simply on the basis of the low probability for it to be extrinsic, although we cannot exclude its association to the neighbour galaxy detected by *HST* (Chen et al., 2007). In that case, it should be realized that the comparatively low H I column density reported by Fynbo et al. (2005) would be the sum of the H I column of the two galaxies, such that they both have even lower H I columns.

3.2. The near-IR emission lines

Assuming a redshift of the host of $z = 2.3351$ (Møller et al. 2002b, based on Lyα emission) we searched the ISAAC spectra for redshifted lines of H I (Hα, Hβ) and [O III] (4,959 Å/5,007 Å). There are tentative detections at low significance of Hα and the [O III] lines. In order to confirm the reality of the lines we used the method we introduced in Jensen et al. (2001). Briefly the method involves rebinning the spectra into redshifts for the rest wavelength of each expected line, in our case the lines of Hα and [O III] (4,959 Å/5,007 Å). The three "redshift spectra" were then coadded (with weights 2, 1 and 1 because of the slightly higher S/N of the tentative Hα detection). The resulting combined line is clearly detected, as shown in Fig. 4.

To this combined line we fit a Gaussian (overplotted as a blue dotted line) and we measure the systemic redshift to be $z = 2.3304 \pm 0.0005$, which is significantly different from the

values derived from the Lyα emission line (which may be absorbed or modified by resonant scattering) or from the absorption systems (which are affected by the local velocity of the absorbing cloud in the host galaxy). The width of the Gaussian is found to be exactly the spectral resolution, so the lines are unresolved and we can place an upper limit on the intrinsic line width of 600 km s^{-1} FWHM.
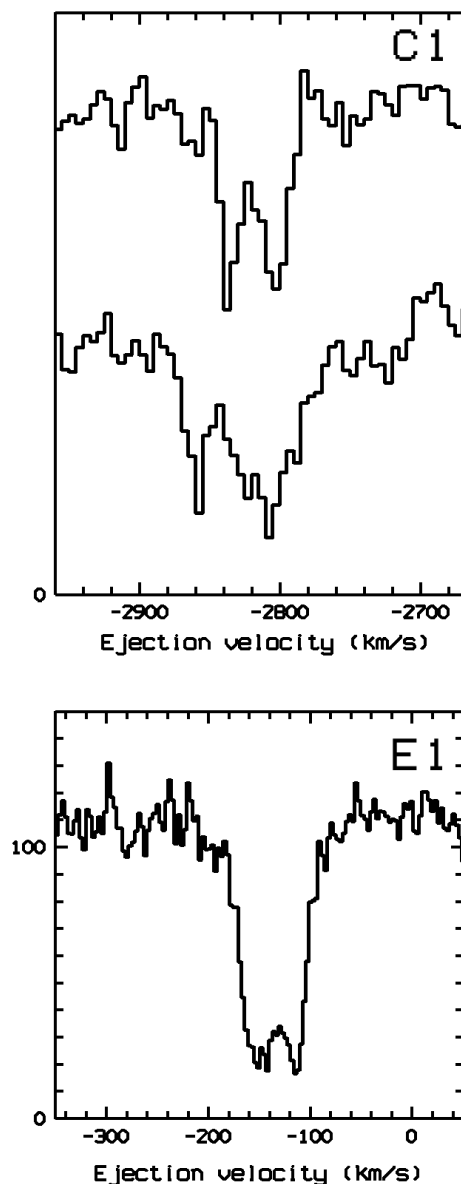

Fig. 3. A zoom in of the high-resolution VLT/UVES spectrum at the location of the C1 and E1 narrow-line absorption systems. The data presented here are the co-add of the different ions in velocity space. Thus, C1 has two subcomponents at 2,803 km s^{-1} and 2,837 km s^{-1} (low ionization, Si II + Al II, top) and 2,810 km s^{-1} and 2,860 km s^{-1} (high ionization, Si III + C IV, bottom). The ionization–velocity correlation also seen in QSOs (Møller et al., 1994) and WR nebulae (Smith et al., 1984) is noticeable. E1 equally splits into two subsystems at 114 km s^{-1} and 150 km s^{-1}. The data shown are the co-add of different ions (N V + Si II + Al II + Al III) in velocity space.
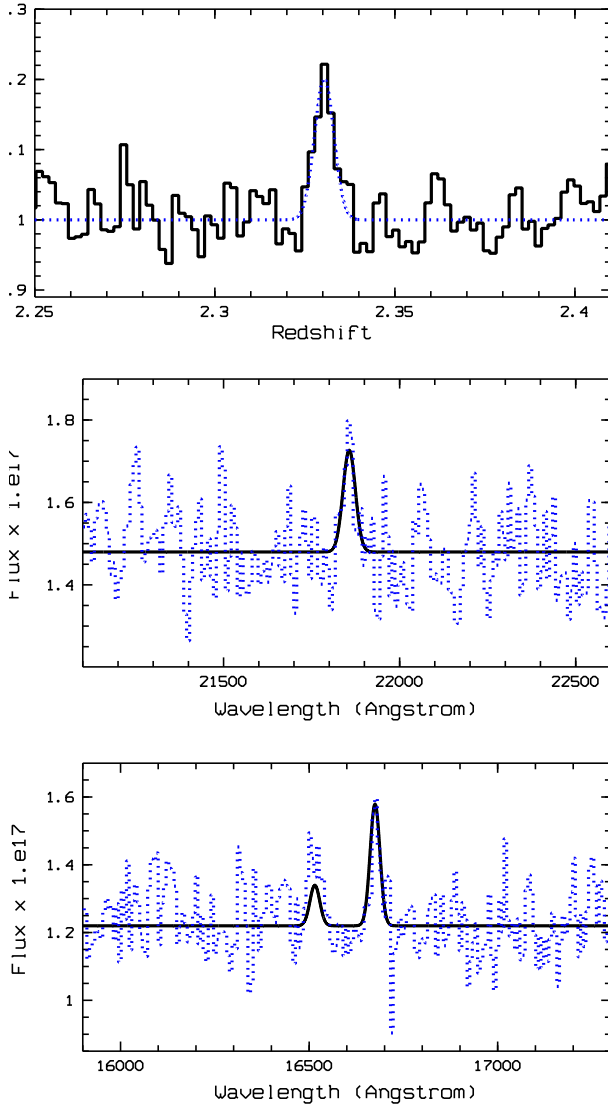
Fig. 4. Bottom panels: A blow-up of the GRB 021004 nIR afterglow spectrum. These VLT/ISAAC data were obtained ~0.6 days after the GRB and show the Hα and [O III] emission lines arising from the host galaxy. Top panel: the co-addition of the three redshift spectra (as explained in the text) is shown, providing an independent measurement of the systemic redshift z = 2.3304 based on the nIR line emission. In the middle and bottom panels we show the optimal fits (black), and the data itself (blue dotted).

Using a redshift of 2.3304 and the width of the resolution profile, we now fitted Gaussian profiles to the data (with continuum level and amplitude of the Gaussian as the only free parameters) using min-square deviation. For the two [O III] lines we further imposed a 1:3 flux ratio (Osterbrock (1989)), we found the following fluxes: flux = $(4 \pm 1) \times 10^{-17}$ erg cm^{-2} s^{-1} ([O III] 4,959 Å), $(12 \pm 3) \times 10^{-17}$ erg cm^{-2} s^{-1} ([O III] 5,007 Å) and $(11 \pm 2) \times 10^{-17}$ erg cm^{-2} s^{-1} (Hα). The Hβ flux is consistent with zero.

4. Discussion

Following the suggestion that there is often a link between long-duration GRBs and core-collapse supernovae (Stanek et al., 2003; Hjorth et al., 2003) as proposed in 1993 (Woosley, 1993) we know that GRBs arise as the end stages of massive-star evolution. As we describe below, the results presented here provide independent evidence for a massive star ($\geq$ 40 M$_\odot$) progenitor and give additional insight into the immediate surroundings and prior evolution of the star leading up to the catastrophic event.

4.1. A LBV / Wolf-Rayet progenitor

The probability that the three absorption systems C1, C2, and D lie in front of the GRB host galaxy as a chance coincidence is very small and can be computed using the number density of intervening C IV absorbers at $1.8 < z < 3.5$ of 1.5 ± 0.2 per unit redshift (Sargent et al., 1998). We find that the probability to find three of them within the redshift range $\Delta z = 0.0337$ spanned by C1, C2, and D is $\sim 10^{-4}$. Fiore et al. (2005) used a similar argument but added the column densities to obtain an even smaller probablility. Like Fiore et al. (2005) we conclude that the absorbers must be intrinsic to the host galaxy. The large blue shift then makes it unlikely that the physical location can be anywhere else than close to the GRB progenitor.

Furthermore, the probability that the C IV 1,550 Å line for complex E falls on top of the C IV 1,548 Å line for complex D and the Lyα line for system C falls on top of the Si III line for system D by chance is small, of order a few percent for each, although difficult to quantify due to the complex profiles. Therefore, it makes sense to seek a physical explanation for the complex structure of the C, D, and E systems.

The multiple absorption line systems found in the spectrum of GRB 021004 are naturally explained by multiple shell structures formed by the stellar winds of a massive progenitor star (Schaefer et al., 2003). Such line-driven winds are expected for very massive stars (Castor et al., 1975; García Segura et al., 1996) that end their lives as Wolf–Rayet stars (WR) (de Koter et al., 1997), after passing through an unstable Luminous Blue Variable (LBV) phase (Langer et al., 1999). Stellar evolution calculations for massive stars predict a number of different phases in which the wind properties associated with those phases, i.e., the velocities and mass-loss rates, become strongly time-varying (Langer et al., 1999; Maeder, 1983). The minimum initial mass for a star to become a LBV is $\sim$ 40 M$_\odot$ (Langer et al., 1994; Maeder and Meynet, 2000). During the course of their evolution, starting as O-class stars (O $\to$ LBV $\to$ WR $\to$ SN), stars have distinct winds in which their velocities are proportional to the escape velocities. Thus, for each transition where a fast wind (i.e., when the stellar radius was small) follows a slow one (larger stellar radius), a shell of swept-up material is formed. Within this simple scheme, computations of the circumstellar medium around a 60 M$_\odot$ star at the zero-age main sequence (García Segura et al., 1996) may produce the number of distinct compressed shells in the kinematic range seen in Fig. 2.
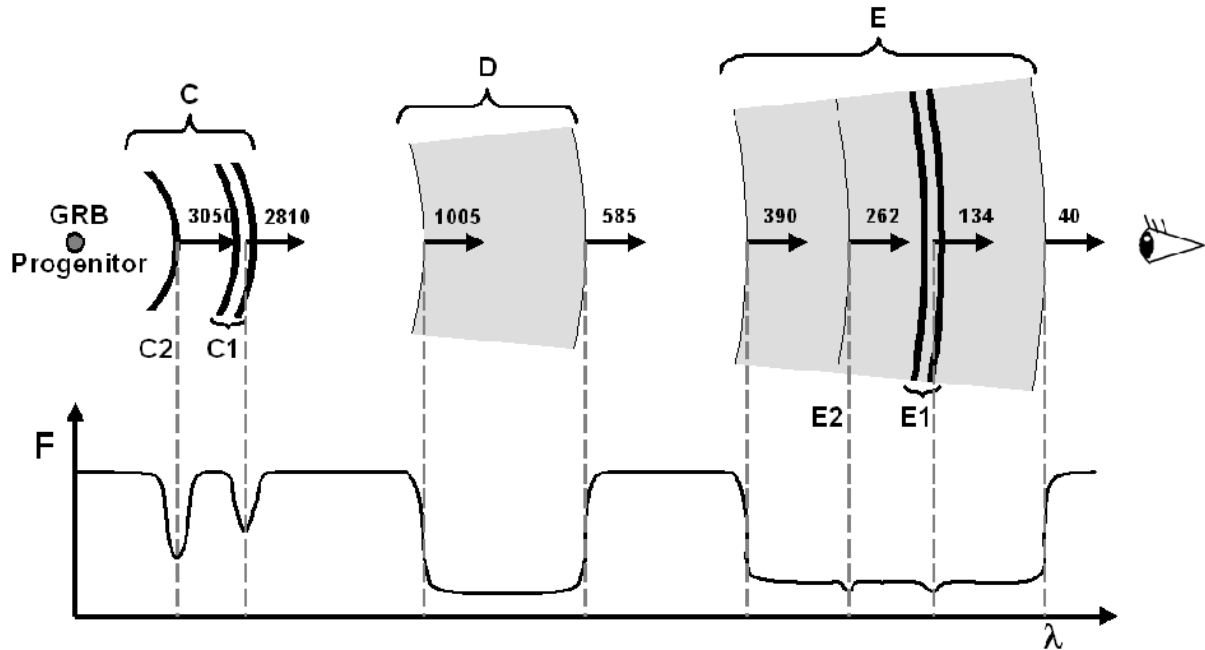
Fig. 5. A sketch showing the absorption line complexes C, D and E in the line of sight to GRB 021004, not drawn to scale. Velocities are given in km s^{-1}. Complex C, with the highest relative velocity, is most likely nearest to the progenitor site in space and probably formed at the WR phase. The high-ionization sub-component C2 is the closest one to the progenitor whereas the colder sub-component C1 is further out and we cannot exclude that it could be even related to the neighbour galaxy detected by *HST* (Chen et al., 2007). Complex E has the lowest relative velocity, and the broad part of the E complex is most likely caused by the oldest wind formed when the progenitor evolved from being an O star into the LBV phase or in the early LBV phase. The narrow E1 component has the properties expected for the ISM of the host galaxy. We believe that the D complex is caused by winds formed during the unstable LBV phase.

During the LBV phase, when hydrogen shell burning occurs, the stellar models are affected by several instabilities that cannot yet be modelled self-consistently and thus the unstable LBV phase can not be fully resolved (Langer et al., 1994). However, several LBV observations show that a number of different swept-up shells can be formed. In particular, the D complex discussed above is akin to the Homunculus nebula around η Car, which contains ~ 1 M$_\odot$ and expands in the range 700 and 1,000 km s^{-1} (Humphreys and Davidson, 1994). As the formation of each of these swept-up shells occurs when the LBV reaches the Eddington limit (Langer et al., 1999), massive stars are able to form several compressed shells before ending their lives.

We note that, since the LBV stellar wind is asymmetric and often leads to a bipolar or at least asymmetric nebula (Gruendl et al., 2000), the GRB has to be beamed in the same direction as the wind for us to see the shells in absorption. Similar, but less spectacular, complex absorption has been detected in GRB 030226 (Klose et al., 2004, but see Shin et al. 2006) and GRB 050505 (Berger et al., 2006); this effect is not seen, however, in several other cases with similar quality data (Chen et al., 2007). It is possible, therefore, that GRBs where no such complex velocity structure is seen have a different orientation of the wind and GRB jet. Highly ionized gas ($\sim T = 10^5$ K) like C IV, N V or Si IV, similar to that found in the environment of GRB 021004, has already been reported

in a number of galactic ring nebulae surrounding Wolf-Rayet stars (Boronson et al., 1997). To form such gas shells, forward shocks with $\sim 10^2$ km s^{-1}, or reverse shocks with $\sim 10^2$–10^3 km s^{-1} are required. The most natural explanation for the C complex is that it has been formed at the WR phase, with C1 and C2 lying in an expanding free wind, before reaching the shocked stellar wind. In fact, the ionization-velocity correlation seen in the systems C1 and C2 has also been detected in WR nebulae, but at lower velocities (~ 100–150 km s^{-1}; Smith et al. 1984).

In addition to the detailed picture of the spatial and velocity structure of the GRB progenitor star at the time of explosion (Fig. 5) our observations have also provided insight into the physical mechanism producing the progenitor shell structure. The fact that the C1 and C2 profiles are not P-Cygni, but almost symmetric profiles, rules out that they are very close to the burst (within ~ 0.2 pc) and being accelerated by the GRB ionizing flux to the observed velocities, as has been proposed elsewhere (Schaefer et al., 2003; Mirabal et al., 2003). The detected line-locking also favours radiative acceleration by the progenitor star.

4.2. A starburst host galaxy

An extremely blue host galaxy has been revealed in late time imaging (Fynbo et al., 2005; de Ugarte Postigo et al., 2005;

Jakobsson et al., 2005). In order to derive the star-forming rate (SFR), we have studied the emission lines seen in the combined optical-nIR spectrum.

The emission line parameters are measured with a Gaussian fit to the emission line and a flat fit to the continuum. If all the Hα emission is attributed to star formation in the host galaxy we can compute the SFR as SFR (M$_\odot$yr^{-1}) = 7.9 $\times$ 10^{-42} $L_{H\alpha}$ (erg/s) (Kennicut et al., 1994). In our assumed cosmology, the measured Hα intensity transforms into a Hα luminosity $L_{H\alpha}$ = (4.9 $\pm$ 0.9) $\times$ 10^{42} erg s^{-1}. This implies a SFR (without any corrections) of 40 $\pm$ 7 M$_\odot$yr^{-1}, which is much larger than the present-day rate in our Galaxy. From the total measured Lyα intensity (Castro-Tirado et al., 2002), we derive a Lyα luminosity $L_{Ly\alpha}$ $\leq$ (9 $\pm$ 1) $\times$ 10^{42} erg s^{-1}, which implies a SFR $\leq$ 10 M$_\odot$yr^{-1} in agreement with Fynbo et al. (2005) and Jakobsson et al. (2005). The Lyα/Hα ratio of 2 implies a low dust content in the GRB host galaxy, as also inferred by de Ugarte Postigo et al. (2005) and Kann et al. (2006) from the afterglow SED; there is also no excess absorption beyond the (low) Galactic value detected in *Chandra* X-ray observations (Sako & Harrison, 2002a). This is a large value for the SFR (see also Castro-Tirado et al. (2007)), although the signal-to-noise ratio of the nIR spectrum implies a large uncertainty. The derived SFR implies that most of the ongoing star formation is unobscured, which is also in agreement with the SCUBA results at 850 μm (Tanvir et al., 2004).

The Lyα photons produced in the ionized nebula suffer a continuous resonant scattering in the presence of HI. In a dust free nebula this mechanism effectively traps the Lyα photons producing a typical P Cygni line profile in emission and absorption, depending on the details of the density and velocity field. However, if even a little dust is present, most Lyα photons will disappear by heating dust grains, because radiation absorption by dust has a maximum cross section near the wavelength of Lyα. Thus, the observed complex Lyα profile is the result of both mechanisms, resonance scattering which sets the profile shape, and dust absorption which further decreases the intensity of the emission line. The Lyα P Cygni profile can be understood in terms of these mechanisms acting during the evolution of the swept up HI supershell produced by a massive starburst in the host galaxy of GRB 021004. It corresponds to stage 4 in the evolutionary scheme developed by Tenorio-Tagle et al. (1999) and Más-Hesse et al. (2003); an stage compatible with GRB 021004 being the evolution endpoint of a WR star.

5. Conclusions

We find several absorption line groups spanning a range of about 3,000 km s^{-1} in velocity relative to the redshift of the host galaxy. The absorption profiles are very complex with both velocity-broadened components extending over several 100 km s^{-1} and narrow lines with velocity widths of only $\sim$ 20 km s^{-1}. By analogy with QSO absorption line studies, the relative velocities, widths, and degrees of ionization of the lines ("line-locking", "ionization–velocity correlation") show that the progenitor had both an extremely strong radiation field and several distinct mass loss phases (winds). These results are consistent with GRB progenitors being massive stars, such as LBVs or

Wolf–Rayet stars, and provide further insight into the nature of these progenitors and their immediate environments.

The host galaxy is a prolifically star-forming galaxy at a systemic redshift z = 2.3304, with a SFR of $\sim$40 M$_\odot$yr^{-1} as also found by Fynbo et al. (2005) and de Ugarte Postigo et al. (2005), reinforcing the potential association of some GRB with starburst galaxies (Christensen et al. (2004); Gorosabel et al. (2005) and references there in).

The *Swift* mission with a predicted lifetime of ten years (Gehrels et al., 2004) will certainly bring us the opportunity to carry out high-resolution spectroscopy for dozens of future GRBs, and to set physical/chemical properties common to all GRB outflows.

References

Barraud, C., Olive, J.-F., Lestrade, J. P., et al. 2002, A&A, 400, 1021

Berger, E., Frail, D. A., & Kulkarni, S. R. 2002, GCN Circ. 1613, http://gcn.gsfc.nasa.gov/gcn/gcn3/1613.gcn3

Berger, E., Penprase, B. E., Cenko, S. B., Kulkarni, S. R., Fox, D. B., Steidel, C. C., & Reddy, N. A. 2006, ApJ, 642, 979

Bersier, D., Stanek, K. Z., Winn, J. N., et al. 2003, ApJ, 584, L43

Björnsson, G., Gudmundsson, E. H., & Johánesson, G. 2004, ApJ, 615, L77

Bloom, J. S., Perley, D. A., Li, W., et al. 2009, ApJ, 691, 723

Boroson, B., McCray, R., Oelfke Clark, C., et al. 1997, ApJ, 478, 638

Castor, J. I., Abbott, D. C., & Klein, R. I. 1975 ApJ, 195, 157

Castro, S., Galama, T. J., Harrison, F. A., Holtzman, J. A., Bloom, J. S., Djorgovski, S. G. & Kulkarni, S. R., 2003 ApJ, 586, 128

Castro-Tirado, A. J., Pérez, E., Gorosabel, J., et al. 2002, GCN Circ. 1635, http://gcn.gsfc.nasa.gov/gcn/gcn3/1635.gcn3

Castro-Tirado, A. J., Bremer, M., McBreen, S. et al. 2007, A&A 475, 101

Chen, H.-W., Prochaska, J. X., Ramirez-Ruiz, E., Bloom, J. S., Dessauges-Zavadsky, M., & Foley, R. J. 2007, ApJ, 663, 420

Chornock, R., & Filippenko, A. 2002, GCN Circ. 1605, http://gcn.gsfc.nasa.gov/gcn/gcn3/1605.gcn3

Christensen, L., Hjorth, J., & Gorosabel, J., 2004, A&A, 425, 913

de Koter, A., Heap, S. R., & Hubeny, I. 1997, A&A, 477, 792

de Ugarte Postigo, A., Castro-Tirado, A. J., Gorosabel, J., et al. 2005, A&A, 443, 841

de Ugarte Postigo, A., D'Elia, V., Goldoni, P., et al. 2009, A&A, submitted (arXiv:0911.3901)

D'Elia, V., Fiore, F., Perna, R., et al. 2009, ApJ, 694, 332

Dessauges-Zavadsky, M., Chen, H.-W., Prochaska, J. X., Bloom, J. S., & Barth, A. J. 2006, ApJ, 648, L89

D'Odorico, S., Dekker, H., Mazzoleni, R., et al. 2006, in SPIE Conf. Series, Vol. 6269

Fiore, F., D´Elia, V., Lazzati, D., et al. 2005, ApJ, 624, 583

Fox, D. W., Yost, S., Kulkarni, S. R., et al. 2003, Nature, 422, 284

Fox, A. J., Ledoux, C., Vreeswijk, P. M., Smette, A., & Jaunsen, A. O. 2008, A&A, 491, 189

Frail, D. A., & Berger, E, 2002, GCN Circ. 1574, http://gcn.gsfc.nasa.gov/gcn/gcn3/1574.gcn3

Fynbo, J. P. U., Gorosabel, J., Smette, A., et al. 2005, ApJ, 633, 317

García-Segura, G., Mac Low, M.-M., & Langer, N. 1996, A&A, 305, 229

Gehrels, N., Chincarini, G., Giommi, P., et al. 2004, ApJ, 611, 1005

Gorosabel, J., Pérez-Ramírez, D., Sollerman, J., et al. 2005, A&A, 444, 711

Gruendl, R. A., Chu, Y.-H., Dunne, B. C., & Points, S. D. 2000, AJ, 120, 2670

Hjorth, J., Sollerman, P., Møller, P., et al. 2003, Nature, 423, 847

Holland, S. T., Weidinger, M., Fynbo, J. P. U., et al. 2003, AJ, 125, 2291

Humphreys, R. M., & Davidson, K. 1994, PASP, 106, 1025

Jakobsson, P., Björnsson, G., Fynbo, J. P. U., et al. 2005, MNRAS, 362, 245

Jensen, B. L., Fynbo, J. P. U., Gorosabel, J., et al. 2001, A&A, 370, 909

Kann, D. A., Klose, S., & Zeh, A. 2006, ApJ, 641, 993

Kann, D. A., Masetti, N., Klose, S. 2007, AJ, 133, 1187

Kann, D. A., Klose, S., Zhang, B., et al. 2010, ApJ, submitted (arXiv:0712.2186v2)

Kawabata, T., Matsumoto, K., Ayani, K., Kawai, N., Urata, Y, & Yamaoka, H. 2004, IBVS 5576

Kennicutt, R. C., Tamblyn, P., & Congdon, C. E. 1994, ApJ, 435, 22

Klose, S., Greiner, J., Rau, A., et al. 2004, AJ, 128, 1942

Langer, N., Hamann, W.-R., Lennon, M., Najarro, F., Pauldrach, A. W. A., & Puls, J. 1994, A&A, 290, 819

Langer, N., García-Segura, G., & Mac Low, M.-M. 1999, ApJ, 520, L49

Lazzati, D., Rossi, E., Covino, S., Ghisellini, G., & Malesani, D. 2002, A&A, 396, L5

Lazzati, D., Perna, R., Flasher, J., Dwarkadas, V. V., & Fiore, F. 2006, MNRAS, 372, 1791

Maeder, A., & Meynet, G. 2000, A&A, 361, 159

Maeder, A. 1983, A&A, 120, 113

Más-Hesse, J. M., Kunth, D., Tenorio-Tagle, G., et al., *Star Formation through Time*, PASP Conference series, 297, 177, eds.: E. Pérez, R. González-Delgado & G. Tenorio-Tagle

Matheson, T., Garnavich, P. M., Foltz, C., et al. 2003, ApJ, 582, L5

Metzger, M. R., Djorgovski, S. G., Kulkarni, S. R., Steidel, C. C., Adelberger, K. L., Frail, D. A., Costa, E., & Frontera, F. 1997, Nature, 387, 878

Mirabal, N., Halpern, J. P., Chornock, R., et al. 2003, ApJ, 595, 935

Møller, P., Jakobsen P., & Perryman, M. A. C. 1994, A&A, 287, 719

Møller, P., Warren, S. J., Fall, S. M., Fynbo, J. P. U., & Jakobsen, P. 2002a, ApJ, 574, 51

Møller, P., Fynbo, J. P. U., Hjorth, J., et al. 2002b, A&A, 396, L21

Osterbrock, D. E. 1989, *Astrophysics of Gaseous Nebulae and Active Galactic Nuclei*, University Science Books, Mill Valley

Pandey, S., Sahu, D. K., Resmi, L., et al. 2003, Bull. Astro. Soc. India 31, 19

Pooley, G. 2002a, GCN Circ. 1575, http://gcn.gsfc.nasa.gov/gcn/gcn3/1575.gcn3

Pooley, G. 2002b, GCN Circ. 1588, http://gcn.gsfc.nasa.gov/gcn/gcn3/1588.gcn3

Prochaska, J. X., Chen, H.-W., & Bloom, J. S. 2006, ApJ, 648, 95

Prochaska, J. X., Dessagues-Zavadsky, M., Ramirez-Ruiz, E., 2008, ApJ, 685, 344

Salamanca, I., Rol, E., Wijers, R. A. M. J., Ellison, S., Kaper, L., & Tanvir, N., 2002, GCN Circ. 1611, http://gcn.gsfc.nasa.gov/gcn/gcn3/1611.gcn3

Salvaterra, R., Della Valle, M., Campana, S., et al. 2009, Nature, 461, 1258

Sako, M., & Harrison, F. A. 2002a, GCN Circ. 1624, http://gcn.gsfc.nasa.gov/gcn/gcn3/1624.gcn3

Sako, M., & Harrison, F. A. 2002b, GCN Circ. 1716, http://gcn.gsfc.nasa.gov/gcn/gcn3/1716.gcn3

Sargent, W. L. W., Boksenberg, A., & Steidel, C. C. 1988, ApJS, 68, 539

Savaglio, S., Fiore, F., Israel, G., et al. 2002, GCN Circ. 1633, http://gcn.gsfc.nasa.gov/gcn/gcn3/1533.gcn3

Schaefer, B. E., Gerardy, C. L., Höflich, P., et al. 2003, ApJ, 588, 387

Shin, M.-S., Berger, E., Penprase, B. E., et al. 2006, ApJ, submitted (astro-ph/0608327)

Shirasaki, Y., Graziani, C., Matsuoka, M., et al. 2002, GCN Circ. 1565, http://gcn.gsfc.nasa.gov/gcn/gcn3/1565.gcn3

Smith, L. J., Pettini, M., Dyson, J. E., & Hartquist, T. W. 1984, MNRAS 211, 679

Srianand, R., Petitjean, P., Ledoux, C., & Hazard, C. 2002, MNRAS, 336, 753

Stanek, K., Matheson, T., Garnavich, P. M., et al. 2003, ApJ, 591, L17

Starling, R. L. C., Wijers, R. A. M. J., Hughes, M. A., Tanvir, N. R., Vreeswijk, P. M., Rol, E., & Salamanca, I. 2005, MNRAS, 360, 305

Tanvir, N. R., Barnard, V. E., Blain, A. W., et al. 2004, MNRAS, 352, 1073

Tanvir, N. R., Fox, D. B., Levan, A. J., et al. 2009, Nature, 461, 1254

Tejos, N., Lopez, S., Prochaska, J. X., Chen, H.-W., & Dessauges-Zavadsky, M. 2007, ApJ, 671, 622

Tejos, N., Lopez, S., Prochaska, J. X., Bloom, J. S., Chen, H.-W., Dessauges-Zavadsky, M., & Maureira, M. J. 2009, ApJ, 706, 1309

Tenorio-Tagle, G., Silich, S. A., Kunth, D., Terlevich, E., & Terlevich, R. 1999, MNRAS, 309, 332

Thöne, C. C., Greiner, J., Savaglio, S., & Jehin, E. 2007, ApJ, 671, 628

Uemura, M., Kato, T., Ishioka, R., & Yamaoka. H. 2003, PASJ, 55, L31

Vergani, S., D., Petitjean, P., Ledoux, C., Vreeswijk, P., Smette, A., & Meurs, E. V. J. 2009, A&A, 503, 771

Vreeswijk, P. M., Ledoux, C., Smette, A., et al. 2007, A&A, 468, 83

Wang, L., Baade, D., Höflich, P., Wheeler, J. C. 2003, ApJ, submitted (astro-ph/0302166)

Woosley, S. E., Bloom, J. S. 2006, ARA&A, 44, 507

Woosley, S. E. 1993, ApJ, 405, 273

List of Objects

Table 3. Line Identifications in the GRB 021004 OA spectra.

λ_{vacuum}(observed) (Å)	Line ID	EW (Å)[a]	z
4008	H I Lyα 1215.670		2.2967
4015	Si III 1206.499		2.3275
4016	Si III 1206.499		2.3289
4028	C IV 1548.203		1.6024
4038	H I Lyα 1215.670		2.3216
4041	H I Lyα 1215.670		2.3243
4045	H I Lyα 1215.670		2.3275
4047	H I Lyα 1215.670		2.3289
4049[b]	H I Lyα 1215.670		2.3304
4084.0	N V 1238.821	0.46 ± 0.16	2.2967
4097.2	N V 1242.804	0.35 ± 0.15	2.2967
4123.9	N V 1238.821	0.90 ± 0.14	2.3289
4137.2	N V 1242.804	0.66 ± 0.12	2.3289
4158.5	Si II 1260.422	0.25 ± 0.10	2.2993
4195.8	Si II 1260.422	0.71 ± 0.19	2.3289
4210.2	Si II 1264.738	0.51 ± 0.16	2.3289
4347.4	Al II 1670.787	0.49 ± 0.17	1.6020
4399.6	C II 1334.530	0.38 ± 0.15	2.2968
4403.0	C II 1334.530	0.79 ± 0.14	2.2994
4639.7	Si IV 1393.754	1.39 ± 0.83	2.3289
4669.7	Si IV 1402.770	1.29 ± 0.46	2.3289
5104.0	C IV 1548.203	1.77 ± 0.12	2.2967
5107.8	C IV 1548.203	0.16 ± 0.03	2.2992
5108.5	C IV 1548.203	0.84 ± 0.10	2.2998
5112.5	C IV 1550.777	1.15 ± 0.09	2.2967
5116.2	C IV 1550.777	0.06 ± 0.04	2.2992
5117.0	C IV 1550.777	0.67 ± 0.08	2.2998
5138.3	C IV 1548.203		2.3189
5140.0	C IV 1548.203		2.3200
5143.1	C IV 1548.203		2.3220
5146.7	C IV 1550.777		2.3188
5146.7	C IV 1548.203		2.3243
5148.5	C IV 1550.777		2.3200
5148.5	C IV 1548.203		2.3255
5151.7	C IV 1550.777		2.3220
5152.9	C IV 1548.203		2.3275+2.3289
5155.2	C IV 1550.777		2.3243
5157.6	C IV 1550.777		2.3255
5161.5	C IV 1550.777		2.3275+2.3289
5235.4	Si I 1572.718	0.80 ± 0.10	2.3289
5559.5	Al II 1670.787	0.23 ± 0.07	2.3275
5561.9	Al II 1670.787	1.73 ± 0.12	2.3289
5578.0	Fe II 2344.214	1.01 ± 0.15	1.3796
5651.2	Fe II 2374.461	0.52 ± 0.06	1.3800
5652.4	Fe II 2374.461	0.16 ± 0.05	1.3805
5652.9	Fe II 2374.461	0.13 ± 0.02	1.3807
5671.2	Fe II 2382.765	0.86 ± 0.07	1.3801
5671.9	Fe II 2382.765	0.41 ± 0.06	1.3804
5672.6	Fe II 2382.765	0.37 ± 0.06	1.3807
6099.6	Fe II 2344.214	0.59 ± 0.04	1.6020
6101.7	Fe II 2344.214	0.28 ± 0.04	1.6029
6154.5	Fe II 2586.650	0.67 ± 0.08	1.3794
6155.0	Fe II 2586.650	0.50 ± 0.09	1.3798
	Fe II 2365.552	0.50 ± 0.09	1.6020
6174.2	Al III 1854.716	1.15 ± 0.09	2.3289
6178.0	Fe II 2374.461	0.52 ± 0.08	1.6020
6187.0	Fe II 2600.173	0.67 ± 0.10	1.3794
6187.5	Fe II 2600.173	0.44 ± 0.08	1.3798
6188.0	Fe II 2599.147	0.50 ± 0.09	1.3808
6201.0	Al III 1862.790	0.73 ± 0.12	2.3289
6202.0	Fe II 2382.765	0.94 ± 0.16	1.6028
6654.0	Mg II 2796.352	1.95 ± 0.11*	1.3796
6655.5	Mg II 2796.352	1.95 ± 0.11*	1.3802
6657.0	Mg II 2796.352	0.71 ± 0.08	1.3808
6671.0	Mg II 2803.531	1.89 ± 0.41*	1.3796
6673.0	Mg II 2803.531	1.89 ± 0.41*	1.3802
6729.0	Fe II 2586.650	0.25 ± 0.07	1.6016
6730.2	Fe II 2586.650	0.60 ± 0.07	1.6020
6732.5	Fe II 2586.650	0.18 ± 0.06	1.6029
6764.0	Fe II 2600.173	0.56 ± 0.10	1.6015
6765.5	Fe II 2600.173	0.71 ± 0.09*	1.6020
	Fe II 2599.147	0.71 ± 0.09*	1.6030
6768.0	Fe II 2600.173	0.46 ± 0.09	1.6029
6788.0	Fe II 2607.866	0.14 ± 0.05	1.6030
7274.2	Mg II 2796.352	1.11 ± 0.10	1.6015
7275.5	Mg II 2796.352	0.83 ± 0.08	1.6020
7277.0	Mg II 2796.352	0.44 ± 0.07	1.6025
7278.5	Mg II 2796.352	0.83 ± 0.08	1.6029
7293.0	Mg II 2803.531	0.89 ± 0.09	1.6015
7294.5	Mg II 2803.531	0.98 ± 0.09	1.6020
7296.0	Mg II 2803.531	0.24 ± 0.06	1.6025
7297.0	Mg II 2803.531	1.00 ± 0.10	1.6029
7803.7	Fe II 2344.214	0.71 ± 0.28	2.3289
7931.8	Fe II 2382.765	0.46 ± 0.21	2.3288
16520[c]	[O III] 4960.295	-(16 ± 7)	2.3304
16679[d]	[O III] 5008.240	-(21 ± 6)	2.3304
21863[e]	H I 6564.610	-(37 ± 10)	2.3304

[a] Gaussian profile fitting (for non saturated lines only). Star symbols refer to complex systems.

[b] Emission line. Partially absorbed, Lyα flux = $(1.5 \pm 0.2) \times 10^{-16}$ erg cm^{-2} s^{-1}.

[c] Emission line.[O III] flux = $(4 \pm 3) \times 10^{-17}$ erg cm^{-2} s^{-1}.

[d] Emission line.[O III] flux = $(12 \pm 3) \times 10^{-17}$ erg cm^{-2} s^{-1}.

[e] Emission line. Hα flux = $(11 \pm 2) \times 10^{-17}$ erg cm^{-2} s^{-1}.